THE 'CAMP' CAMPAIGN 1982

E Kopp[1], F Bertin[2], L G Björn[3], P HG Dickinson[4], C R Philbrick[5] & G Witt[6]

[1] *Physikalisches Institut, University of Bern, Switzerland*
[2] *CRPE, 94107 Saint-Maur des Fossés, France*
[3] *Swedish Space Corporation, Solna, Sweden*
[4] *Rutherford Appleton Laboratory, Chilton, Didcot, Oxon, UK*
[5] *AFGL, Hanscom AFB, MA 01731, USA*
[6] *Meteorological Observatory, Stockholm University, Sweden*

ABSTRACT

The Cold Arctic Mesopause Project (CAMP) was conducted at Esrange, Sweden, in July/August 1982. Seven rockets were launched on August 3/4 during a period of noctilucent cloud (NLC) sighting over Esrange. A second salvo with three rocket launchings occurred on August 11/12 but without a NLC sighting. The presence of NLC on August 3/4 was confirmed by several rocket-borne photometer and plasma probe profiles. The NLC height was 83±1 km. Before and during the main salvo a high magnetic disturbance was present with 1.7 db absorption on the 27 MHz riometer and a -480 nT north-south magnetic field bay. Accordingly high positive ion densities of $2.5 \times 10^5 cm^{-3}$ at 90 km and $1.6 \times 10^4 cm^{-3}$ at 80 km were measured in the lower ionosphere. The temperature measurements showed, that their profiles in the stratosphere and lower mesosphere were near the expected values as predicted by high latitude summer models. At altitudes between 83-94 km a wave structure with three temperature minima of 139 K, 114 K and 111 K was observed. The 138 K temperature minimum was located at the height of the observed NLC. Positive and negative ion composition measurements were obtained from four rocket flights. Atomic oxygen was measured in both salvoes between 65-135 km using resonance fluorescence and absorption at 130 nm. Nitric oxide densities could be inferred from positive ion composition measurements.

Keywords: Middle Atmosphere, Summer Mesosphere, Polar Region, Rocket Campaign

INTRODUCTION

The mesosphere at high latitudes in summer is known to possess the highest clouds of the earth atmosphere, named noctilucent clouds (NLC). Appearances of NLC and their properties have been the subject of numerous investigations in the past. The formation of NLC in the summer arctic mesosphere is associated with a region having the coldest atmospheric temperatures and regions of super saturated water vapor. The extremely low temperatures of the summer mesopause at high latitudes reflect the special dynamical state of this region. The cooling of the mesosphere is the result of upward vertical air motion in the polar middle atmosphere, which causes adiabatic cooling of the mesosphere. In addition, the relative lack of wave dissipation in summer reduces the stratospheric and mesospheric heating and the downward transport of thermospheric minor constituents, especially atomic oxygen, nitric oxide and carbon monoxide.

During the last eight years two rocket campaigns have been performed at Esrange (lat 67.9N, long 21.4E). The rocket campaigns were instrumented for a study of several atmospheric properties necessary to describe the NLC. In the first campaign (NLC 1978) the first rocket salvo (July 30, 1978 /1/) gave new information on the chemistry of the summer arctic mesopause and on the formation mechanism for NLC particles by ion nucleation. The second campaign, which took place in summer 1982 at Esrange, was part of the MAP project CAMP (Cold Arctic Mesopause Project), /2,3/. The rocket measurements in CAMP were supported by ground based, airplane and satellite remote sensing experiments. Of special importance for CAMP was the UV-backscatter experiment on the SME satellite /4/ which, during summer 1982, gave a continuous survey of the polar mesospheric clouds (PMC) at NLC heights over the summer polar cap region. The rocket borne techniques in CAMP included optical photometers to detect NLC particles, mass spectrometers for positive and negative ion species, high resolution electron and total positive ion probes, accelerometer measurements of density, temperature and wind, chemical release wind measurements, ionization rates from solar and particle sources, and minor species such as atomic oxygen and argon.

In this paper a selection of rocket and ground based measurements at the time of the first salvo (3/4 Aug) in CAMP will be presented (Table 1).

Proceedings of the 7th ESA Symposium on European Rocket & Balloon Programmes and Related Research, Loen, Norway, 5-11 May 1985 (ESA SP-229, July 1985).

Table 1: Selected Measurements of CAMP in Salvo A, Aug 3/4 1982

Rocket Payload	Instrument	Parameter	Date (UT)	Time	Experimenter
	EISCAT	Vertical Wind	Aug 2	23.00	F. Bertin
CAMP-P	Mass Spectrometer	Positive Ion Composition	Aug 3	23.32	E. Kopp
CAMP-P	Ion Probes	Positive Charge, Aerosol	Aug 3	23.32	L.G. Björn
SOAP 1	Photometer Lyman-α	NLC-height Temperature	Aug 3	23.49	G. Witt
SOAP 1	Resonance Fluorescence	Atomic Oxygen	Aug 3	23.49	P.H.G. Dickinson G. Witt
P235K	Resonance Fluorescence	Atomic Oxygen	Aug 4	00.05	P.H.G. Dickinson
TAD	Active Falling Sphere	Temperature, Density, Wind Velocity, Turbulence, Waves	Aug 4	00.16	C.R. Philbrick
SU-LO	Thermistor	Temperature	Aug 4	00.31	C.R. Philbrick

MEASUREMENTS

Measurements in CAMP were obtained from a total of ten rocket payloads launched in two salvoes. The main salvo (salvo A) with seven rockets started at 23.02 UT on August 3 and the smaller salvo (salvo B) with three rockets began at 23.30 UT on August 11, 1982. Details of the different payloads and instruments have been published by Björn (1984) /2/. Salvo A was launched into a developed and stable NLC display observed from the spotter aircraft 500 km south of Esrange over the period of the seven rocket launches. The altitude of NLC observed with rocket borne photometers and positive ion probes was 83±1 km. This salvo was launched only a few days after a major solar proton event, which had caused much larger electron and ion densities than originally anticipated. Fig. 1 and Fig. 2 give measurements of the north-south magnetic field and the riometer absorption at 27 MHz in Kiruna during salvo A on Aug 3/4. High electron densities of $5 \times 10^3 cm^{-3}$ at 80 km and $3 \times 10^5 cm^{-3}$ at 100 km were measured as a consequence of the high ionization rate. The advantage of the high ionization was the good signal/noise ratio obtained with incoherent scatter radar echoes from EISCAT (the European Incoherent Scatter Radar at Tromsö, Kiruna and Sodankylä), which made the measurement of vertical wind velocities possible.

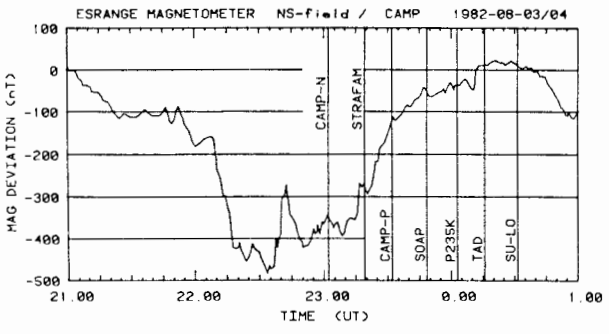

Fig. 1. North-south magnetic field deviation recorded at Esrange during salvo A of CAMP, Aug 3/4. The times of the launchings of the different payloads are indicated by vertical bars.

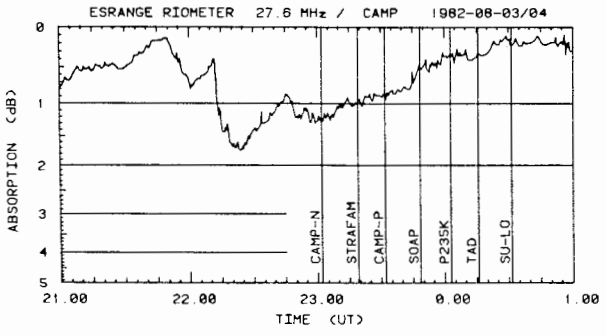

Fig. 2. Esrange 27 MHz riometer absorption recorded at Esrange during salvo A of CAMP, Aug 3/4.

Six optional photometers were used on the payloads CAMP-N, CAMP-P and the SOAP (Selective Optical Atmosperic Probe) payloads in salvo A for the detection of the NLC layer. Fig. 3 gives the intensity of the scattered sunlight as measured with a photodiode sensor in the visible wavelength range. The photodiode had a narrow field of view to the side of the payload. Two curves are shown with different rocket spin phase angles. The enhancement above the normal Rayleigh scattered light of the background atmosphere at 81-83 km originated from the presence of visible NLC particles. The other photometers on CAMP-P and CAMP-N have also detected the scattered light from the NLC layer at similar heights. On the CAMP-P payload the positive charge density was measured with a spherical probe consisting of an inner sphere with 1.7 cm and an outer grid with 4 cm diameter, respectively. The grid was biased with -5V relative to the rocket ground and the accelerating potential between grid and sphere was 10V.

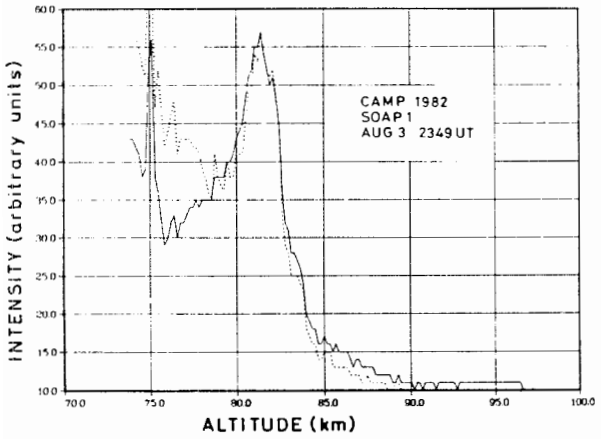

Fig. 3. The intensity of visible radiation detected by a side looking photodiode photometer on SOAP 1 rocket payload as a function of altitude. The two profiles were obtained at two selected rocket spin phases. The large signals found at 82.6. km are diagnostics of NLC.

The derived positive charge density in Fig. 4 has been calibrated against the electron density measurement at about 95 km from the propagation experiment on the same payload. The ascent and descent profile of the boom probe in Fig. 4 is scaled down by a factor of ten for better comparison with profiles from the current to the conical tip of the mass spectrometer. This indicates the total positive charge impinging on the outer surface. The bias of the unguarded MS-tip probe is -3V on rocket ascent and -10V on descent. The surface area of the tip probe is approximately 50 cm^2. This probe was flown on the same payload as the boom probe (CAMP-P). It reveals a distinct positive charge layer at the height of NLC during rocket descent (e.g. Fig. 4). The fact, that this layer is not observed with the boom probe suggests, that this layer is caused by positively charged aerosols of unknown size, for which the boom probe has a much lower cross section.

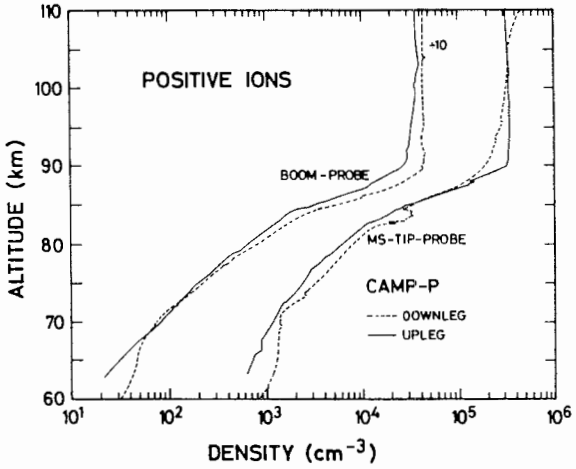

Fig. 4. Positive charge density profiles measured on CAMP-P payload. The density derived from the gridded boom probe is divided by 10. The positive charge density derived from the current of the open conical shaped tip probe of the mass spectrometer reveals a distinct layer on the rocket descent at an altitude of 83.0 km.

The cross section presented to the positive charges entering the grid on the boom probe is mass and mobility dependent. The current to the inner sphere on the boom is mostly attributed to the standard ions in the mass range 10-100 u. The cross section for heavy ions and charged aereosols is much larger on the MS-tip probe. A contribution of photoemission at both probes by Lyman-α radiation is possible (1 and 5×10^{-10}A, respectively at 85 km altitude). The observed increase of positive charge current on descent of CAMP-P is, however, not explainable by an enhancement of the photoemisssion from scattered Lyman-α at NLC-particles with a Zenit angle $\chi = 94°$. The reason that positively charged aerosols can exist, can only be explained with a faster photodetachment process compared to the time for electron loss by attachment to these particles in the sunlit polar mesosphere. The photodetachment cross section depends on the particle size and the nature of the aerosols (heterogeneous or homogeneous particles) and it is therefore quite possible that zones with mainly negatively charged aerosols can also exist, even in a sunlit mesosphere.

In situ measurements of temperature were made in salvo A using measurements of density by falling accelerometer sphere /5/, bead termistor measurements of temperature /6/ and scale height temperature measurements from absorption of Lyman-α sunlight and EISCAT /15/. The four temperature profiles are given in Fig. 5. The temperature profile of the stratosphere obtained from the meteorological Super-Loki flight (Su-Lo) is in good agreement with the Air Force Reference Atmosphere for 75°N and August /7/. The temperature profile between 55 and 120 km of Fig. 5 was derived from the high resolution density measurement of the triaxial accelerometer on the TAD payload.

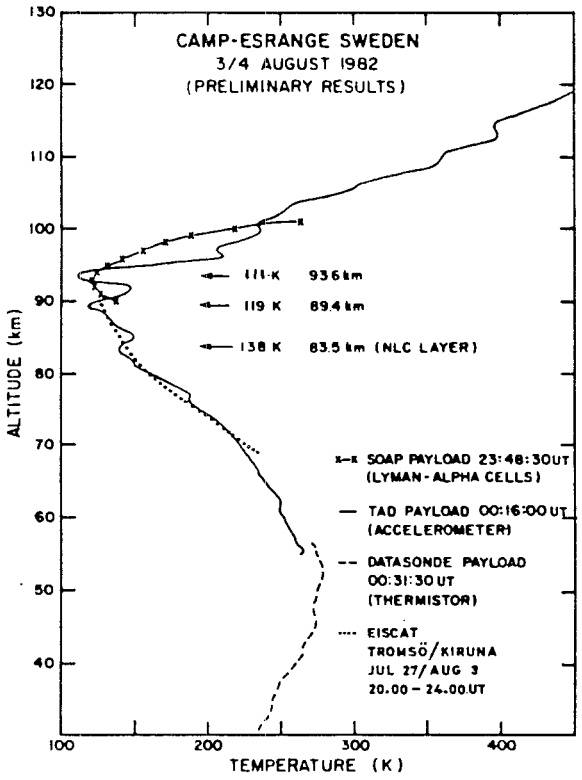

Fig. 5. Comparison of four temperature profiles obtained during the NLC display on 3/4 August in salvo A.

The wave structure between 80-100 km has three temperature minima, 139 K at 83.5 km, 119 K at 89.4 km and 111 K at 93.6 km altitude. The first minimum is located at the NLC height. The temperatures of the two latter minima are significantly lower than any which have been previously measured in the atmosphere. The lowest temperatures previously measured at the summer high latitude mesopause over Pt. Barrow (71°N) /8/ with grenades were 130-140 K. The grenade technique did not have sufficient altitude resolution to resolve temperature structures of 5-7 km vertical wavelength as observed in CAMP at the mesopause. A temperature profile determined from integrating the profile of the molecular absorption UV-measurement (Lyman-α) on the SOAP payload was obtained between 90 and 100 km (e.g. Fig. 5). The temperature from the Lyman-α technique is derived assuming hydrostatic equilibrium and does not have sufficient height resolution to resolve the temperature wave observed with the triaxial accelerometer. The results of the Lyman-α measurement gave a temperature minimum of about 120 K in the vicinity of 93 km. The mean temperature profile obtained from the width of the incoherent scatter spectra (EISCAT) agrees with the average temperature from the triaxial accelerometer in the height range 68-90 km.

The wave structure found in the temperature profile is much more pronounced in the zonal wind velocity of Fig. 6. The mean zonal wind, as determined from the triaxial accelerometer on the TAD payload, is westward below 94 km and eastward above, in good agreement with the models /9/ and ground based radar measurements /10/. A well developed gravity wave with five vertical wavelengths was measured in the zonal wind at 65-98 km with a mean vertical wavelength of 7.5 km. The exponential growth of the amplitude with increasing height is evident only at heights below 70 km. The gravity wave above 70 km is affected by dissipation by 5 turbulent layers found at 75.5 km, 79.5 km, 86.5 km, 89 km, and 93 km. The presence of five turbulent layers is seen in the calculated profile of the potential temperature derived from the accelerometer temperature measurements of salvo A. The negative gradient of the potential temperature (e.g. Fig. 6) indicates dynamically unstable layers. The region 75-93 km with five turbulent layers is typical of the height region where the MST radar echoes above Poker Flat have maximum signal to noise ratios in summer /11/.

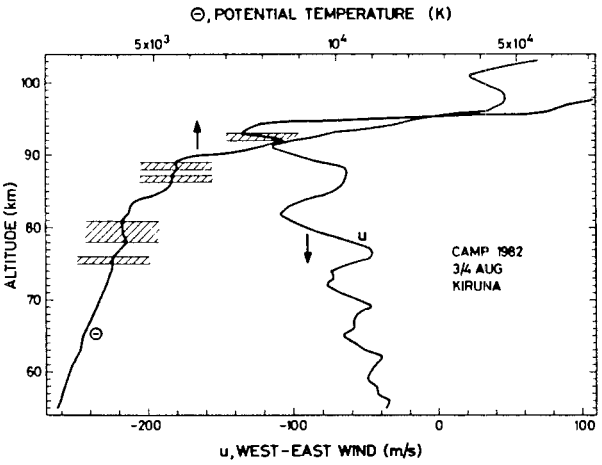

Fig. 6. Profiles of the potential temperature and zonal wind velocity measured with the triaxial piezoelectric accelerometer on the TAD payload in salvo A. 5 regions with negative potential temperature gradients indicate the presence of turbulent layers.

Vertical wind amplitude measurements are available from the EISCAT measurement on Aug. 2 around 2300 UT the evening before salvo A was launched (Fig. 7). Error bars and relative time in minutes with respect to 2300 UT are marked at each measured value. The measurements by EISCAT were made in the bistatic mode. By using the envelope around the measured wind velocities, an amplitude range of ±5 m/s can be estimated for the vertical wind perturbation w'. In Table 2 a set of the relevant gravity wave parameters is given. A horizontal wavelength of about 45 km is calculated from the ratio of horizontal (30 m/s) to vertical (5 m/s) wind amplitude and the vertical wave length of about 7.5 km.

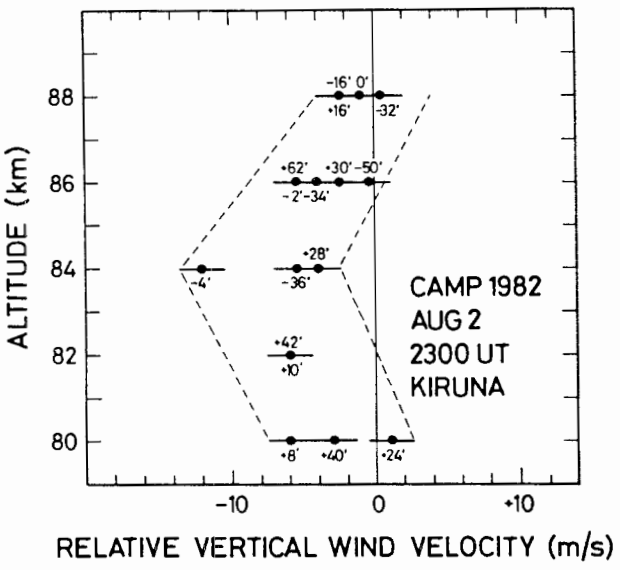

Fig. 7. Vertical wind velocities measured in the evening of Aug 2, with EISCAT. The minutes relative to 2300 UT and the error bars are indicated on the measured value. The amplitude of the vertical wind perturbation w' is about 5 m/s. The sign of the wind velocities is arbitrary and is not associable to upward or downward transport.

Table 2: Gravity Wave Parameters of Salvo A in CAMP, Aug 3/4

Parameter	Measurement	Experiment
Zonal Wind u'	≅ 30 m/s	Active Falling Sphere
Vertical Wind w'	≅ 5 m/s	EISCAT
Vertical Wavelength λ_z	≅ 7.5 km	Active Falling Sphere EISCAT
Horizontal Wavelength λ_x	≅ 45 km	$u'/w' = \lambda_x/\lambda_z$
Wave Period	≅ 30 min	EISCAT

Fig. 8 gives the result of two atomic oxygen measurements in salvo A of CAMP. The measurements were obtained by using rocket borne UV resonance lamps /12/. On the Petrel (P235K) payload measurements were made of resonance fluorescence and absorption using the $OI(^3P_j - ^3S_1)$ triplet at 130 nm. The experiment on SOAP payload measured resonance fluorescence only. The Petrel ascent profile shows the atomic oxygen concentration over the full altitude range 60-140 km (e.g. Fig. 8).

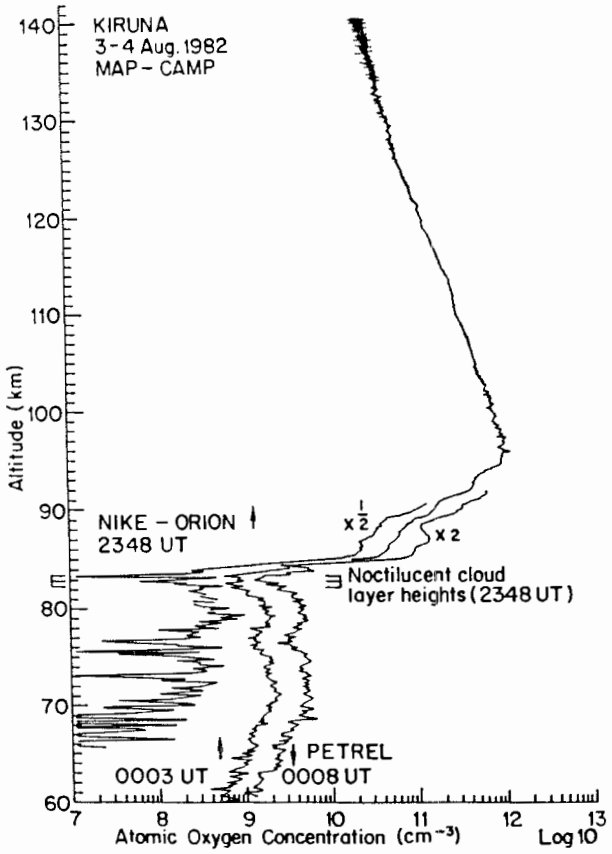

Fig. 8. Atomic oxygen concentrations measured in salvo A by resonance fluorescence and absorption at 130 nm (Petrel) and resonance fluorescence (SOAP). The ascent profile of the Petrel experiment covers the full height range. The descent part of the Petrel is scaled up in concentration normalized to the Petrel profile at about 90 km is shown with a concentration scaled down by a factor of two. At NLC heights (indicated with markers) all three profiles have minimum counts.

The descent part of the Petrel measurement is scaled up by a factor of two. The measurement from the SOAP payload is only shown below 90 km, with a factor of two reduction in concentration for better separation of the profiles. The SOAP profile was normalized to the Petrel profile at 90 km. Above 90 km the atomic oxygen concentration on SOAP and on descent of Petrel were perturbed by vehicle related effects and are not given in Fig. 8. At the altitude of NLC all three oxygen profiles have a count minimum. A possible local enhancement of the water vapor and the odd hydrogen mixing ratio at the NLC height caused from the evaporation of water ice, could explain the depression of atomic oxygen by reactions:

$$O + OH \rightarrow H + O_2 \qquad (1)$$

$$O + HO_2 \rightarrow OH + O_2 \qquad (2)$$

If the reactions (1) and (2) of atomic oxygen with odd hydrogen species are the dominant loss processes in the vicinity of NLC an increase of the odd hydrogen concentration of a factor of 2-3 would have been present during CAMP at the NLC height. The atomic oxygen concentration had a density decrease from $10^{12}cm^{-3}$ at 94 km to a very low value of $6x10^{9}cm^{-3}$ at 84 km. This gradient can be attributed to chemical loss reactions with odd hydrogen and weak vertical transport from the thermosphere to the mesosphere. The different layers with stable and unstable dynamical behavior and variable mixing ratios of water vapor and odd hydrogen were probably responsible for some of the small scale structures observed in the atomic oxygen profile.

Fig. 9 gives the profiles of positive ions measured on the ascent of the CAMP-P payload with the magnetic ion mass spectrometer /13/. The ions were sampled through an orifice of 2 mm diameter at the apex of the conical shaped MS-tip at an attracting potential of -3V on ascent and -10V on descent. A mass range of 14-280 u was analyzed. The absolute positive ion densities were determined by normalizing at 90-95 km to the electron density measured on the same payload by the propagation technqiue. At the NLC height the total proton hydrate density reached its maximum value. The highest order proton hydrates - $H^+(H_2O)_7$ - were also measured at 82-83 km altitude. The narrow depression of the metal ion density profile at 94 km altitude is at the height of the sharp zonal wind reversal (e.g. Fig. 6). The depression may be caused by the combined effect of the zonal wind shear and the small horizontal component of the earth magnetic field, causing vertical migration of the ions away from the shear height. The positive ion composition measurement was used to infer the nitric oxide concentration in Fig. 10, above 91 km, the height where the loss of O_2^+ with NO in the reaction

$$O_2^+ + NO \rightarrow NO^+ + O_2 \qquad (3)$$

is not negligible /14/. The nitric oxide concentration decreases, from $8x10^{8}cm^{-3}$ at 100 km to $2.5x10^{7}cm^{-3}$ at 90 km. The steep NO gradient is explained, like that as for the atomic oxygen, by weak vertical transport from the thermosphere to the mesosphere and additional chemical loss with odd hydrogen in reaction.

$$NO + HO_2 \rightarrow OH + NO_2 \qquad (4)$$

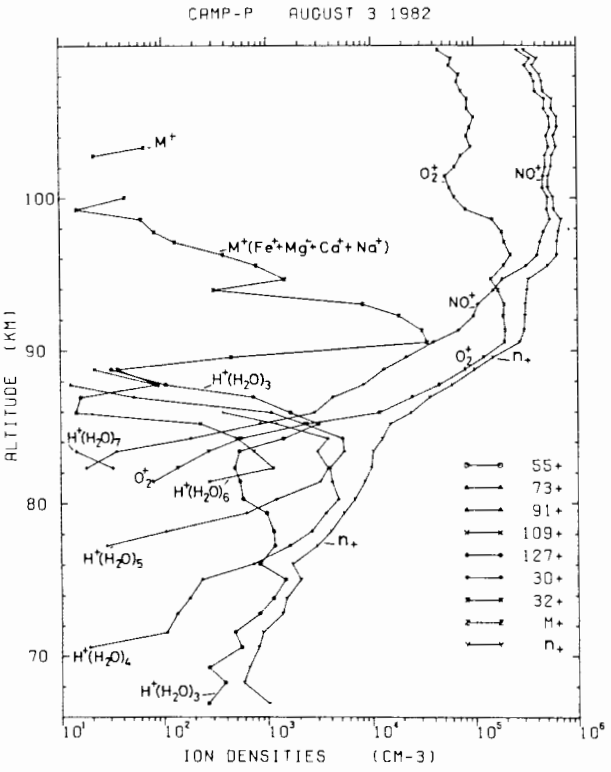

Fig. 9. Positive ion density profiles measured on ascent of CAMP-P payload in salvo A. The absolute densities were normalized to the electron density measured by propagation experiments on the same payload at 90-95 km. The measured density profiles of cluster ions O_2^+X and NO^+X are not shown. At the NLC height, the proton hydrate concentrations were largest and also the highest order proton hydrate density - $H^+(H_2O)_7$ was measured.

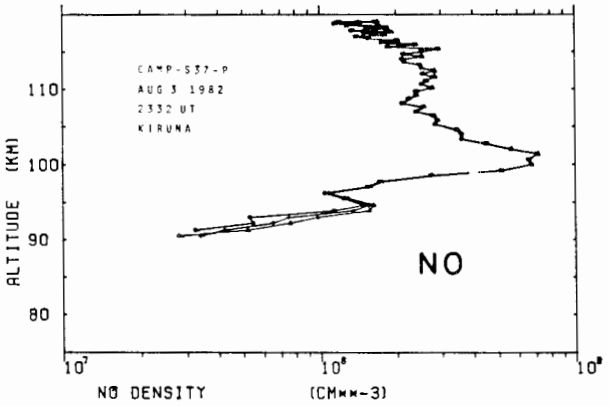

Fig. 10. Nitric oxide concentration inferred from the positive ion composition measurements on CAMP-P in salvo A.

CONCLUSIONS

At the observed height of visible NLC (83±1 km) several features as summarized in Table 3 were observed: local loss of atomic oxygen, a local temperature minimum, positively charged aerosols and a large concentration of proton hydrates including the highest order of proton hydrate.

In situ temperature and wind measurements and EISCAT vertical wind measurements revealed five thin layers of turbulence in the mesosphere between 75 and 93 km and the presence of a gravity wave with a vertical wavelength of 7.5 km. The observed turbulent layers will dissipate the gravity waves. The region of wave dissipation is shifted from 50-70 km in winter to 75-90 km altitude range in summer.

Table 3: Events at the NLC-height

Payload	Parameter	Altitude
CAMP-P	Positively Charged Aerosol Layer	83.7 km Ascent 83.0 km Descent
	Highest Order and Maximum Density of Proton Hydrates	82 ± 0.5 km
SOAP 1	NLC-Photometers	82.4 km lower NLC 83.0 km upper NLC
	O-Density Depression	83.3. km
Petrel	O-Density Depression	83.0 km Ascent and Descent
TAD	First Temperature Minimum	83.5 km

The decrease of atomic oxygen and nitric oxide density at the summer high latitude mesopause indicates the transition from a region above where the lifetimes are determined by transport to the region below with much lower chemical lifetimes for O and NO compared with the time scale for downward transport from the thermosphere.

ACKNOWLEDGEMENT

The CAMP Campaign was supported by: the Swedish Space Corporation (SSC), Solna; The Bundesministerium für Forschung und Technologie (BMFT), Bonn through the DFVLR/BPT, Köln; The Science Research Council (SRC), London; the Swiss National Science Foundation, Bern; the U.S. Air Force Geophysical Laboratory (ASFC), Bedford; the founder of EISCAT: Suomen Akatemia, Helsinki; Centre Nationale de la Recherche Scientifique, Paris; Max-Planck-Gesellschaft, Germany; Norges Almenvitenskapelige Forskningsråd, Norway; Naturvetenskapeliga Forskningsrådet, Stockholm; the Science and Engineering Research Council, UK. We would like to thank K. Torkar and M. Friedrich for their help in evaluating the Faraday rotation measurement. Special thank is indebted to Therese Feller for typing the manuscript.

REFERENCES

1. Björn L G, Kopp E, Herrmann U, Eberhardt P, Dickinson P H G, Mackinnon D J, Arnold F, Witt G, Lundin A and Jenkins D B, Heavy ionospheric ions in the formation process of noctilucent clouds, J. Geophys. Res., in press, 1985.

2. Björn L G, The cold summer mesopause, Adv. Space Res. 4, 4, 145-151, 1984.

3. Björn L G, Cold arctic mesopause project (CAMP) scientific objectives, in middle atmosphere program handbook 4, Ed. C F Sechrist, Jr., Univ. of Illinois, p 161, 1982.

4. Thomas G E, Solar Mesosphere Explorer measurements of polar mesospheric clouds (noctilucent clouds), J. Atmos. Terr. Phys. 46, 819, 1984.

5. Philbrick C R, Fair A C, Fryklund D H, Measurements of atmospheric density at Kwajalein Atoll, May 18, 1977, AFGL-TR-78-0058 Air Force Surveys in Geophysics 384, Air Force Geophysics Laboratory, Hanscom AFB, MA. 01731, U.S.A.

6. Schmidlin F J, Philbrick C R, Offermann D, Atmospheric density, temperature, and wind measurement techniques during the 1980 Energy Budget Campaign, in: BMFT-FB-W 81-052, Ed. D Offermann and E V Thrane, University of Wuppertal, BRD.

7. Philbrick C R, Barnett J, Grendt R, Offermann D, Pendelton Jr. W R, Schlyter P, Schmidlin J F and Witt G, Temperature measurements during the CAMP program, Adv. Space Sci. 4, Nr. 4, 153-156, 1984.

8. Theon J S, Nordberg W, Katchen L B, and Horvarth J J, Some observations on the thermal behavior of the mesosphere, J. Atmos. Sci. 24, 428, 1967.

9. Garcia R R and Solomon S, The effect of breaking gravity waves on the dynamics and chemical composition of the mesosphere and lower thermosphere, J. Geophys. Res. 90, 3850-3868, 1985.

10. Nastrom G D, Balsley B B and Carter D A, Mean meridional winds in the mid- and high-latitude summer mesosphere, Geophys. Res. Let. 9, 139, 1982.

11. Balsley B B, Ecklund W L and Fritts D C, VHF echoes from the arctic mesosphere and lower thermosphere Part I: Observations, in book: Dynamics of the middle atmosphere, Ed. J R Holton and T Matsuno, Terra Scientific Publ. Co., p. 77-96, 1984.

12. Dickinson P H G, Bain W C, Thomas L, Williams E R, Jenkins D B and Twiddy N D, The determination of the atomic oxygen concentration and associated parameters in the lower ionosphere, Proc. R. Soc. Lond. A369, 379-408, 1980.

13. Kopp E, Ramseyer H and Björn L G, Positive ion composition and electron density in a combined auroral and NLC event, Adv. Space Res. 4, No. 4, 157-161, 1984.

14. Grossmann K U, Frings W G, Offermann D, André L, Kopp E, Krankowsky D, Concentrations of H_2O and NO in the mesosphere and the lower thermosphere at high latitudes, J. Atmos. Terr. Phys. 47, 291-300, 1985.

15. Kofman W, Bertin F, Röttger J, Cremieux A and Williams P J S, The EISCAT mesospheric measurements during the CAMP campaign, J. Atmos. Terr. Phys. 46, 565-575, 1984.